On radiative transfer in water spray curtains using the Discrete Ordinates Method

— **Source link** ⧉

Anthony Collin, P. Boulet, David Lacroix, G. Jeandel

Institutions: Centre national de la recherche scientifique

Published on: 15 Apr 2005 - Journal of Quantitative Spectroscopy & Radiative Transfer (Pergamon)

Topics: Radiative transfer, Atmospheric radiative transfer codes and Heat transfer

Related papers:

- Radiative heat transfer

- Numerical modeling of radiative heat transfer in water sprays

- Radiative and conductive heat transfer in a nongrey semitransparent medium. Application to fire protection curtains

- Heat transfer through a water spray curtain under the effect of a strong radiative source

- Fire protection: Water curtains

On radiative transfer in water spray curtains using the Discrete Ordinates Method

Anthony Collin, Pascal Boulet, David Lacroix, Gérard Jeandel

On radiative transfer in water spray curtains using the

Discrete Ordinates Method

A. Collin, P. Boulet[*], D. Lacroix & G. Jeandel

Laboratoire d'Energétique et de Mécanique Théorique & Appliquée (LEMTA), CNRS UMR 7563

Faculté des Sciences et Techniques BP 239 - 54506 VANDOEUVRE Cedex

Tel & Fax (33) 383 684 686 - mail Pascal.Boulet@lemta.uhp-nancy.fr

Keywords : *Radiative transfer, absorption, scattering, water spray, transmissivity*

Abstract

Radiative transfer through water spray curtains has been presently addressed in conditions similar to devices used in fire protection systems. The radiation propagation from the heat source through the medium is simulated using a 2D Discrete Ordinates Method. The curtain is treated as an absorbing and anisotropically scattering medium, made of droplets injected in a mixing of air, water vapor and carbon dioxide. Such a participating medium requires a careful treatment of its spectral response in order to model the radiative transfer accurately. This particular problem is dealt with using a correlated-K method. Radiative properties for the droplets are calculated applying the Mie theory. Transmissivities under realistic conditions are then simulated after a validation thanks to comparisons with some experimental data available in the litterature. Owing to promising results which are already observed in this case of uncoupled radiative problem, next step will be to combine the present study with a companion work dedicated to the careful treatment of the spray dynamics and of the induced heat transfer phenomena.

Nomenclature

- d, droplet diameter (m)

- D_m, radiative source term in the discretized RTE

---

[*]corresponding author

- f_v, droplet volume fraction (m^3 of water/m^3 of spray)

- f_y, f_z, weights for the spatial differencing scheme

- H, height of the medium (m)

- L, width of the medium (m)

- $I_\lambda^0(T)$, blackbody spectral intensity at temperature T ($W.m^{-3}.sr^{-1}$)

- I_λ, spectral intensity ($W.m^{-3}.sr^{-1}$)

- $\dot{m}$, nozzle mass flow rate ($kg.s^{-1}$)

- n_d, number of discrete directions

- n, nozzle density number (m^{-1})

- P, pressure (atm)

- P_λ, spectral scattering phase function

- $\vec{q_r}$, radiative flux ($W.m^{-2}$)

- r, droplet radius (m)

- s, position in the medium (m)

- T, temperature (K)

- T_λ, spectral transmissivity

- $\overline{T}$, total transmissivity

- V_d, mean droplet velocity ($m.s^{-1}$)

- V_C, cell volume (m^3)

- w_m', weight of the quadrature scheme

- x, y, z, space co-ordinates

greek symbols

2

- ϵ_m, correction parameter in the phase function renormalization

- κ_λ, spectral absorption coefficient (m^{-1})

- ρ, density $(kg.m^{-3})$

- σ_λ, spectral scattering coefficient (m^{-1})

- τ, optical depth

- $\vec{\Omega}$, propagation direction

- Ω, solid angle (sr)

  subscripts

- C, N, S, E, O, marks for the cell faces and its center

- g, gas phase property

- d, droplet property

- j, property for the jth quadrature point

- m, direction index

- Δy, Δz, grid size in y and z directions

- λ, spectral property

- μ_m, ξ_m, direction cosines

- ν, property at a given wavenumber

1   Introduction

Originally used in the field of chemical protection due to demonstrated depollution abilities, water spray curtains have been also studied for a long time as possible solutions involved in fire protection systems. In this case, the expected aim is to protect given devices from strong irradiation, due to flames for example. The physical phenomena responsible for such an ability are well-known : absorption and scattering due to water droplets

and vapor result in an attenuation of the incoming radiation. However, accurate modelling of the involved interactions between radiation and the spray is not so easy to achieve. Yet, optimization of the spray efficiency would be a useful tool for people concerned with fire protection. Our group is involved in this task. In particular, the present paper is a study exclusively dedicated to the radiative part of the modelling. A fine solution has been sought, that could accurately deal with the problem of interaction between thermal radiation and water sprays and that could be also easily combined with other aspects of the problem : global heat transfer and dynamics of the spray.

Some of previous works have been dedicated to this problem of sprays used as fire protection systems. Simple calculation models have been first developed in order to compute transmissivity levels directly. Such an approach is sometimes still applied, as in Coppalle *et al.* [1]. Realistic optical properties of water are introduced in the calculation, scattering and absorption efficiencies are computed applying the Mie Theory, but the transmissivity is finally predicted from a two-flux model. Due to the inability of this formulation to take into account acute anisotropic scattering, the predicting efficiency of such an approach cannot be sufficient. Dembélé *et al.* [2] rigorously investigated the suitability of two-flux models for simulating possible attenuation by sprays, comparing their predicting ability with a more elaborate solution based on a Discrete Ordinates Method (DOM). Their conclusion is that two-flux approaches should be generally avoided, unless being in very restricted conditions combining an optically thin medium, very small droplets and a diffuse irradiation.

Studies carried out in the frame of the so-called ASTRRE project have contributed to improve the predicting capacity of numerical models. Pretrel [3] developed a complete one-dimensional description of the dynamics of the spray combined with a thermal model. However, the radiative part of the heat exchanges was still based on a two-flux analysis. Dembélé [4] introduced a more rigorous treatment of the radiative transfer computing radiative properties from the Mie theory and introducing them in a DOM-type code, still in one-dimensional configuration. Note that he also applied a carefull treatment of the spectral variation problem on the basis of a correlated-K model. Numerical results were compared with experimental data of transmissivity measured in laboratory conditions and with more realistic tests under fire conditions, the radiative transfer problem being addressed uncoupled from the rest of the spray modelling. The refinement of the radiative approach yielded promising results especially concerning the spectral variations of the transmissivity. However, there is a lack of results concerning the description of radiation attenuation in sprays really taking into account the whole problem of combined mass, momentum and heat transfer. Moreover, formulations should be extended to 2D or

3D descriptions.

More recently Zimmer [5] presented a complete study of the dynamics of a water curtain, especially addressing effects associated to a possible lateral wind, which has been proven to distort the spray and disperse the droplets. Its work again recalls the need for a multi-dimensional description.

Finally, Berour *et al.* [6] presented a 2D analysis of the heat transfer in the spray, taking into account combined conductive and radiative transfer and thus obtaining very high temperature levels. Introduction of supplementary phenomena such as convection due to droplet fall and air, turbulence effects and droplet evaporation would probably lead to lower temperature levels, due to heat loss increase. Although already based on a DOM-type scheme, its radiative model was planned to be further improved, in so far that it used a basic band model for the spectral treatment and did not account for phase function renormalization for example.

The radiation-spray interaction problem has been often studied uncoupled from the rest of the spray characterization. Even in this case, the formulation is all but simple and some of the difficulties are to be recalled here:

- the medium is a multiphase suspension, flowing due to droplet injection,

- the resulting spray has a non-gray absorbing, emitting and anisotropically scattering behaviour (with a very strong forward scattering peak),

- spectral properties exhibit very sharp variations in given wavelength bands,

- the spray is a polydispersion with droplet diameters ranging in such a large domain that their attenuation ability strongly varies,

- numerous non-radiative factors may affect the spray behaviour (temperature, moisture, volume fraction, surrounding air...).

Despite those uncertainty sources our purpose here has been to develop a better radiative description of the problem, involving up-to-date submodels addressing the various identified difficulties. A predicting tool has been developped. It is a 2D description where external conditions are fixed. Main features of the corresponding model are :

- 2D Discrete Ordinates Method,

- all droplet radiative properties computed from the Mie theory (even the phase function, generally approximated using an analytical function like the Henyey and Greenstein one, which is not the case here, a renormalization process being also performed to ensure the radiative balance),

- spectral dependance of the vapor properties assessed using a correlated-K model involving the database by Soufiani *et al.* [7], with either 43 or 367 wavelength bands,

- various possible quadrature schemes tested (S_N-type, LCN-type and DCT-type),

- various possible spatial differencing schemes tested (STEP or diamond scheme, Carlson-Lathrop scheme [8]).

A companion work is also carried out in parallel in order to ensure the coupling with the global heat, momentum and mass exchanges. In the following sections, the problem formulation will be given and the most useful

details will be recalled on the way radiative properties are calculated. Key difficulties such as the phase function renormalization or the spectral treatment will be in particular discussed. The complete simulation will then provide results for transmissivity features of spray curtains. First of all, a validation of the model will be presented comparing our numerical results with experimental data by Dembélé [4]. The corresponding numerical simulations will concern one-dimensional situations with collimated irradiation, requiring very fine angular discretization schemes. Afterwards, applications to diffuse irradiation in 2D conditions will be discussed. A sensitivity analysis will be also presented, dedicated to the spectral resolution and the various numerical approximations used in the DOM. Finally, complementary numerical data will be discussed, aiming at the description of the behaviour of such media used as fire protection devices. In particular, the influence of droplet size, volume fraction and resulting optical depth will be investigated.

2   Formulation

The main assumptions applied in the present analysis are the following:

- temperature and relative moisture in the medium are constant and set to 300K and 60% respectively (according to available experimental data on those parameters, combined effects due to vaporization and convection actually lead to a temperature level close to the ambient one despite the heat source due to radiative transfer),

- gas and droplets are assumed to have the same temperature (a rigorous two-phase formulation based on coupled energy balances written on each phase would be the only way to avoid this assumption in computing the real temperature levels, which are probably close anyway),

- all volume fractions (for the droplets and the gaseous species) are supposed to remain constant,

- all participating species are assumed to act independently, so that global radiative properties may be obtained by a simple addition of their respective contributions (droplet volume fraction is low enough to consider the hypothesis of independent scattering and carbone dioxide rate is also so small that no combined effects between the gases are to be considered).

The examination of available data in the litterature (especially those by Pretrel [3]) makes the above assumptions reasonable.

2.1 Radiative Transfer Equation

Following the above introductory paragraph, the Radiative Transfer Equation (RTE) for steady-state transfer can be written as follows :

$$\frac{dI_\lambda(s,\vec{\Omega})}{ds} + (\kappa_{d\lambda} + \kappa_{g\lambda} + \sigma_{d\lambda}) I_\lambda(s,\vec{\Omega}) = \kappa_{d\lambda}.I_\lambda^0(T_d(s)) + \kappa_{g\lambda}.I_\lambda^0(T_g(s)) +$$
$$\frac{1}{4\pi} \int_{\Omega'=4\pi} \sigma_{d\lambda}.P_\lambda(\vec{\Omega'} \to \vec{\Omega}).I_\lambda(s,\vec{\Omega'})d\Omega' \tag{1}$$

$I_\lambda(s,\vec{\Omega})$ is the spectral intensity at a given position s in the direction $\vec{\Omega}$, at wavelength λ, $I_\lambda^0(T(s))$ is the spectral blackbody intensity at temperature T (the subscripts d or g refer to the droplet phase or to the gas). The required radiative properties are the droplet spectral absorption coefficient ($\kappa_{d\lambda}$), the droplet spectral scattering coefficient ($\sigma_{d\lambda}$), the corresponding spectral scattering phase function ($P_\lambda(\vec{\Omega'} \to \vec{\Omega})$) and the gas phase spectral absorption coefficient ($\kappa_{g\lambda}$). The formulation of those properties will be discussed in the next paragraph and in appendix A.

In what concerns the emission terms, two temperature levels are still involved here, but as above-mentionned a common assumption will be used considering that both phases are in equilibrium and are therefore at the same temperature. Note that the square of the refractive index is not involved here, considering the very low volume fractions of the various species (around 10^{-5} for the droplets and less than 4.10^{-4} at ambiant temperature for H_2O and CO_2) a value of 1 would be introduced as the best approximation for this parameter, which would

induce no modification for the emission.

Boundary conditions have to be introduced in order to make the formulation complete. Transparent boundaries are assumed at all sides of the problem. On the face irradiated by the main source (the flame side), collimated or diffuse irradiation may be taken into account, depending on the test case (simulation of an indoor experiment involving a collimated source or simulation of realistic fire conditions). There, a blackbody radiation at high temperature is considered. On the other sides the incoming radiation is supposed to be diffuse, corresponding to a blackbody at surrounding temperature.

2.2   Radiative properties computed from the Mie theory

Complete description of this part of the work may be found in Berour *et al.* [6]. For a sake of brievety, let us just recall here that they are computed on the basis of the characteristics of isolated particles, assuming independent scattering. Therefore properties are simply added, taking into account the granulometric distribution of the droplets.

Considering $N(r).dr$ as the density number of droplets having a radius between r and $r + dr$ per cubic meter, the formulation of the various involved variables is as follows:

$$\kappa_{d\lambda} = \int_0^\infty \pi.r^2.Q_{a\lambda}(r).N(r).dr \tag{2}$$

$$\sigma_{d\lambda} = \int_0^\infty \pi.r^2.Q_{s\lambda}(r).N(r).dr \tag{3}$$

$$P_\lambda(\theta) = \frac{1}{\sigma_{d\lambda}} \int_0^\infty \pi.r^2.Q_{s\lambda}.P_\lambda(r,\theta).N(r).dr \tag{4}$$

where the properties of individual particles (absorption and scattering efficiencies ($Q_{a\lambda}$ and $Q_{s\lambda}$) and the scattering phase function for a given droplet size in a given direction $P_\lambda(r,\theta)$) are the exact application of the Mie Theory, as formulated for example by Modest [9]. For the completeness of the present communication, a brief presentation of the way these properties may be computed is proposed in an appendix A at the end of the paper.

Note that the exact formulation of the phase function is used here, instead of replacing this parameter by a simpler formulation based on an analytical approximation as often done. Considering the fact that such

properties are computed once for all as a pre-processing task, we preferred to use the complete Mie formulation to avoid any inaccuracy and build a complete and exact database.

Due to the need of discretization of the RTE, aimed at the reformulation of its integral term (as will be shown later), the continuity of the phase function versus the scattering angle may not be preserved. The consequence is a possible degradation of the numerical implementation of the phase function, which could be no more normalized. Consequently, in case of strong anisotropic scattering, the radiative balance may not be guaranted. Let $P_\lambda(m', m)$ represent the discretized form of the phase function $P_\lambda(\Omega', \Omega)$, expressing the scattering from the m' direction towards the m direction. The normalization process would require that:

$$\frac{1}{4\pi} \int_{\Omega'=4\pi} P_\lambda(\Omega', \Omega).d\Omega' = 1 \tag{5}$$

This integral (which is of course valid after the application of the Mie solution) is replaced by a summation involving n_d directions and featuring integral weight w_m, that will be unable to exactly verify the condition. In other words, we will have the inequality:

$$\frac{1}{4\pi} \sum_{m'=1}^{n_d} w_{m'}.P_\lambda(m', m) \neq 1 \tag{6}$$

This may become a source of strong inacurracy in the case of huge anisotropic scattering (which is our case here). This problem may be avoided applying a renormalization process. Following El Wakil [10] the phase function is modified, considering a parameter ϵ_m aimed at the correction of the phase function involved in the m direction. Consequently the discretized form of the previous equation becomes:

$$\frac{1}{4\pi} \sum_{m'=1}^{nd} w_{m'}.(1 + \epsilon_m + \epsilon_{m'}).P_\lambda(m', m) = 1 \tag{7}$$

This gives us a system of n_d linear equations with solutions corresponding to the correction factors, which is simply solved in a matrix form applying a Gaussian elimination. Finally, the corrected phase function, avoiding any problem of radiative transfer non-conservation, becomes:

$$P_\lambda^*(m', m) = (1 + \epsilon_m + \epsilon_{m'}).P_\lambda(m', m) \tag{8}$$

This pre-processing treatment has been applied before all our simulations.

The gaseous phase has been previously described as an absorbing medium with sharp wavelength variations. This difficulty is addressed in the next paragraph devoted to the spectral treatment, applying a so-called c-K model.

2.3 Use of a c-K model

Radiative transfer in participating gaseous atmospheres has received much attention in more severe conditions than the one expected in the present study. In particular, temperature levels are supposed to be relatively low, and only CO_2 and H_2O vapors will be considered with low volume fractions, at atmospheric pressure. Though, a finer model than a simple large band one will be introduced to describe the attenuation of radiation. A correlated-K model with a seven point Gaussian quadrature scheme has been chosen. This ensures a good accuracy for the spectral description of the medium properties, without leading to a severe increase in the required computational ressources. This method is actually not the most accurate one, but it presents at least two main advantages: it can yield averaged values for the absorption coefficient (whereas some more accurate methods, like the statistical-narrow-band or the line-by-line models, lead to transmissivity values which cannot be directly introduced in the RTE) and it has been proven to be reasonnably fast and robust. The input data by Soufiani and Taine [7] have been used. This reference gives all required explanations on the way the model may be applied and also reports test cases that have been presently used to validate the calculations of transmissivities for mixtures involving H_2O and CO_2. Rather than recalling all the theoretical background of the c-K model, we give hereafter the useful relations applied in our numerical treatment.

The key parameter is $g(k)$ the cumulative distribution function of the pseudo absorption coefficient k, simply defined owing to the near isothermal conditions as: $\kappa = f.P.k$, where f is the gas volume fraction and P the pressure. By definition, we have:

$$g(k) = \int_0^k f(k').dk' \tag{9}$$

where $f(k_\nu)$ is the distribution function of the coefficient k_ν which may be written, according to the Malkmus formulation as:

$$f(k_\nu) = \frac{1}{k}.\sqrt{\frac{\overline{k_\nu}.\overline{\gamma_\nu}}{\pi.k.\overline{\delta_\nu}}}.exp\left[\frac{\overline{\gamma_\nu}}{\overline{\delta_\nu}}.(2 - \frac{k}{\overline{k_\nu}} - \frac{\overline{k_\nu}}{k})\right] \tag{10}$$

In this equation, data must be introduced for the variables $\overline{k_\nu}$ and $\overline{\delta_\nu}$ which are spectral parameters given in [7] on the basis of line-by-line calculations. Two spectral resolutions are available, the first one is based on a constant band width of 25 cm^{-1} (and will be hereafter referred as the "367 band model") whereas the second contains 43 irregular bands and has been built in order to optimize the computation, reducing the calculation time (model hereafter referred as the "43 band model"). The remaining parameter $\overline{\gamma_\nu}$, called the mean half width, is then computed as a function of pressure, temperature and gas volume fraction.

The treatment of the integrals over a given spectral width is performed numerically thanks to a seven point quadrature scheme involving in a classical manner the following quadrature points g_j 0, 0.155405848, 0.45, 0.744594152, 0.9, 0.935505103, 0.984494897 and the corresponding weights ω_j 0.045, 0.0245, 0.32, 0.245, 0.056111111, 0.051248583, 0.037640306. The above-written integral for $g(k)$ therefore becomes:

$$\int_0^{k_j} f(k').dk' = g_j \tag{11}$$

allowing the k_j to be found applying a SIMPSON formulation for the integral computation for example. Consequently, the RTE has to be rewritten in a form involving these coefficients:

$$\frac{dI_j(s,\vec{\Omega})}{ds} + (\kappa_{d\lambda} + \kappa_j + \sigma_{d\lambda})\, I_j(s,\vec{\Omega}) = (\kappa_{d\lambda} + \kappa_j)\,.I_\lambda^0(T(s)) + \frac{1}{4\pi}\int_{\Omega'=4\pi} \sigma_{d\lambda}.P_\lambda(\vec{\Omega'} \to \vec{\Omega}).I_j(s,\vec{\Omega'})d\Omega'$$

where I_j is a value corresponding to the k_j point and with $\kappa_j = k_j.f$ (f being the volume fraction of the species of interest: H_2O or CO_2). No additional correction is needed for the pressure, since our applications are performed at atmospheric pressure. Note that interactions between species are not considered here, owing to the fact that CO_2 will always be involved at very low volume fraction, so that a single additivity is supposed to be valid between the radiative properties of the different species.

The averaged intensity is finally computed as:

$$\overline{I_\nu} = \sum_{j=1}^{7} w_j.I_j(s,\Omega) \tag{12}$$

The main drawback is that the RTE will have to be solved 7 times the number of bands for each iteration, which will increase the computational time. However, the model will produce realistic averaged values for each wavelength band. On the contrary, a simple band model would give an arbitrary spectral value, supposed to be representative of the whole band, whatever the possible spectral variations at the inside.

3 Numerical handling

3.1 DOM scheme

The Discrete Ordinates Method is presently used in a classical way, aimed at the direct solution of the RTE as above-written. The method first introduced by Chandrasekhar [11], further developed by Carlson and Lathrop [8] among others, has been widely applied in similar configurations. The recent formulation presented in Lacroix *et al.* [12] has been used here.

Two main steps have to be considered in the application of the DOM. First of all, a quadrature scheme is applied in order to transform the scattering integral term in a discretized summation involving n_d directions, as follows:

$$\int_{\Omega'=4\pi} \sigma_{d\lambda}.P_\lambda(\vec{\Omega'} \to \vec{\Omega}).I_\lambda(s,\vec{\Omega'}).d\Omega' = \sum_{m'=1}^{n_d} \sigma_{d\lambda}.P_\lambda(m' \to m).I_\lambda(s,m').w_{m'} \quad (13)$$

The sensitivity of results to some available quadrature schemes is discussed in the next paragraph. The RTE is therefore rewritten as:

$$\frac{dI_j(s,m)}{ds} + (\kappa_{d\lambda} + \kappa_j + \sigma_{d\lambda}) I_j(s,m) = (\kappa_{d\lambda} + \kappa_j).I_\lambda^0(T(s)) +$$
$$\frac{1}{4\pi} \sum_{m'=1}^{n_d} \sigma_{d\lambda}.P_\lambda(m' \to m).I_j(s,m').w_{m'} \quad (14)$$

[Figure 1 about here.]

Afterwards this equation has to be integrated on a control volume V_C as drawn on figure 1, where the notations are given for the intensity at various locations in and around the cell. In a two-dimensional configuration in the yz plane, introducing the direction cosines μ_m and ξ_m, the RTE becomes :

$$\int_{V_C} \xi_m.\frac{dI_j}{dy}.dy.dz + \int_{V_C} \mu_m.\frac{dI_j}{dz}.dy.dz + \int_{V_C} (\kappa_{d\lambda} + \kappa_j + \sigma_{d\lambda}).I_j.dy.dz = \int_{V_C} D_m(y,z,m).dy.dz \quad (15)$$

with

$$D_m(y,z,m) = (\kappa_{d\lambda} + \kappa_j).I_\lambda^0(T(s)) + \frac{1}{4\pi}.\sum_{m'=1}^{n_d} \sigma_{d\lambda}.P(m' \to m).I_{j,C}(y,z,m').w_{m'} \quad (16)$$

Considering constant radiative properties on a control volume, applying a discretization in space and dividing by the cell volume $(\Delta y.\Delta z)$, it yields:

$$\frac{\mu_m}{\Delta z}.[I_{\lambda,E}(y,z,m) - I_{\lambda,O}(y,z,m)] + \frac{\xi_m}{\Delta y}.[I_{\lambda,N}(y,z,m) - I_{\lambda,S}(y,z,m)]$$
$$+(\kappa_{d\lambda} + \kappa_j + \sigma_{d\lambda}).I_{\lambda,C}(y,z,m) = D_m(y,z,m) \quad (17)$$

This expression is the formulation of the RTE obtained with the Discrete Ordinates Method. Owing to the knowledge of the intensity at the boundaries of the problem and to the sweeping of the computational domain, the intensity is known upstream from point C. For example, starting from the south-west corner, the intensities

will be unknown at the north and east sides. Closure equations have to be introduced to obtain the intensity at the opposite sides of the cell, such that:

$$I_{\lambda,C}(y,z,m) = f_z.I_{\lambda,O}(y,z,m) + (1-f_z).I_{\lambda,E}(y,z,m) = f_y.I_{\lambda,S}(y,z,m) + (1-f_y).I_{\lambda,N}(y,z,m) \qquad (18)$$

The scheme used to compute f_y and f_z may influence the results. This point is addressed in the next paragraph.

3.2   Quadrature and differencing scheme influence

Among the numerical approximations required in the DOM formulation, two are discussed here : the quadrature scheme and the differencing scheme. The classical S_N quadrature has been widely used in numerical treatments like the present one. The S_8 quadrature is for example often introduced, corresponding to a split of the whole space in 80 directions (only 40 would be considered here due to a symmetry property relative to the yz plane). Based on a recent review proposed by Koch and Becker [13], other quadratures have been tested. In particular, comparisons have been carried out and will be presented in the "validation" section, between computations performed with a S_{12} scheme (168 directions) and cases referred as $LC11$, $DCT111 - 24681012$ and $DCT020 - 2468$ in the above-mentioned review (in the followings, they will be only abreviated as $DCT111$ and $DCT020$). This choice was done since the $LC11$ was presented by Koch and Becker as the most accurate one when tested against its ability to reproduce the first order moment (with a discretization according to 120 directions), whereas the $DCT111$ and the $DCT020$ were presented as very good compromises between accuracy and computational effort leading to a reasonable error while only using 80 and 48 directions respectively.

For the spatial differencing scheme, a well-known formulation by Carlson and Lathrop [8] has been generally applied in the present study :

$$f_y = \max\left(f_y', \frac{1}{2}\right) \text{ with } f_y' = 1 - \frac{\Delta z}{\frac{\Delta y}{|\xi_m|}\left[(\kappa_{d\lambda} + \kappa_j + \sigma_{d\lambda})\Delta z + 2|\mu_m|\right]} \qquad (19)$$

$$f_z = \max\left(f_z', \frac{1}{2}\right) \text{ with } f_z' = 1 - \frac{\Delta y}{\frac{\Delta z}{|\mu_m|}\left[(\kappa_{d\lambda} + \kappa_j + \sigma_{d\lambda})\Delta y + 2|\xi_m|\right]} \qquad (20)$$

As a complement, a sensitivity analysis has been also carried out, comparing the results with others obtained with simpler schemes like the "diamond" scheme ($f_y = f_z = 1/2$) and the "step" scheme ($f_y = f_z = 1$).

3.3   Numerical processing

Since the size distribution of the spray is known (see reference [4] for the input data of the applications hereafter referred "TG03 - 1 bar" and "TG03 - 3 bars"), the radiative properties for the droplets can be computed for

each wavelength band. Then, introducing the temperature and the volume fractions for H_2O and CO_2, the c-K model gives the absorption coefficient of the continuous phase at each quadrature point for all wavelength bands. Afterwards, the RTE is solved applying the DOM technique. Typically, in the present applications, a spatial grid of 80x30 cells was sufficient to obtain mesh-independent results. The reference solution used a $DCT111$ quadrature and a spectral discretization on 367 or 43 bands.

Successive sweepings of the domain, starting from each of the four corners, were performed. Convergence was tested on the basis of normalized residuals calculated on the intensities integrated over the whole spectral range. Computations were stopped when the sum of all variations on each node, in each direction, between two successive loops, was found smaller than 10^{-16} (actually the computer limitations).

4   Validation

A first validation has been performed, testing the ability of the present code to simulate the transmissivity of a spray as a function of the wavelength. Comparisons have been carried out with the experimental data by Dembélé [4]. The numerical conditions are the following : the spray is referred as "TG03 - 1 bar", completely described in what concerns the size distribution in the above-mentioned reference, with droplet diameters ranging from 10 to around 170 μm, with a mean Sauter diameter of 100.5 μm (hereafter noted D_{32} and defined by relation (22)) and a calculated droplet concentration of 8.2x10^{-6} m^3 of droplets / m^3 of air, the temperature and the moisture inside the spray are 300K and 60 % respectively. Consequently, the volume fractions for H_2O and CO_2 have been fixed to 2.11x10^{-2} and 2.93x10^{-4} m^3 of gas / m^3 of air respectively.

The width of the spray is 0.24 m. The incoming radiation on the spray corresponds to a collimated source due to a blackbody at 1573K, impinging perpendicularly to the spray boundary. Expected results are the directional spectral transmissivity in the incidence direction. Due to the crucial role of scattering, this problem requires a special quadrature with a very fine accuracy, at least around the incidence direction. In following the complete 2D description of the previous paragraph, this could requires a too huge mesh size and consequently excessive computational ressources. This is why the problem has been first treated as one-dimensional with azimuthal symmetry, in order to evaluate our ability to reproduce the experimental data. (Thereafter, comparisons will be carried out between the one-dimensional analysis and the complete 2D model, to demonstrate its suitability to yield a correct simulation, when diffuse irradiation is considered and hemispherical transmissivity - instead of directional value - is sought). Consequently, the discretization is only applied on the polar angle in the

present case, with a constant but very fine step, set to 0.5 degrees. The step scheme is applied for the spatial differencing scheme, to yield a simple but stable formulation, especially for directions far from the collimated one where negative intensity might be observed with diamond differencing scheme.

Details concerning the pre-processing of the simulation (spectral variations of the optical index for water and corresponding evolution of the radiative properties computed for the droplets, applying the Mie theory) have been widely presented in [6]. We will only focus on transmissivity levels. The previous paragraph reported the way the spectral intensity is calculated through the solution of the RTE. The normal spectral transmissivity in a given wavelength band is then computed as the ratio between the incoming and leaving intensities in the normal direction, at the boundaries of the spray.

Thereafter, integration on the whole wavelength range would yield the total normal transmissvity of the spray. Results are presented in the spectral range $[1.5; 13 \mu m]$ corresponding to the main part of the incoming radiation, where experimental results are available to allow the comparison. Figure 2 presents the corresponding numerical prediction obtained with a spectral discretization according to 367 or 43 bands and the reference experimental data. Note that the experimental curve has been re-built using the figures of reference [4], which may induce some local inaccuracies even if the curve actually is an accurate picture of the original data. As can be seen, sharp variations due to the attenuation by the continuous phase are obtained, which are remarkably reproduced by the numerical simulation. Peaks due to H_2O (at 2.7 μm and around 6.5 μm) and also to CO_2 (at 4.3 μm) are reproduced. Small local discrepancies may be observed in the peak intensities but the agreement is globally very good. Note that the simulation based on 43 bands is also very satisfactory, even if some details are lost in the spectral variations. An averaged transmissivity level of 92% has been obtained numerically (for the two spectral discretization solutions), integrating the spectral results between 1.5 and 13 μm, whereas a value of 90% was cited in the original experimental study. This is a satisfactory agreement bearing in mind possible uncertainties, for example on the exact droplet distribution or on the spray width.

A second test has been performed in similar conditions but with a second spray, thus with a different size distribution, referred as "TG03 - 3 bars" (also completely described in [4], in particular with droplet diameters ranging from 10 to around 230 μm, with a mean Sauter diameter of 101.1 μm and a calculated droplet concentration of 24.2x10^{-6} m^3 of droplets / m^3 of air). Results are plotted on Figure 3. As can be seen, here again the agreement is satisfactory. The spectral behavior is similar, but due to different droplet characteristics the global attenuation is better. Actually, the increase in pressure provides smaller droplets with a higher global

concentration. Smaller droplets are known to enhance the scattering ability of the spray, with a decrease of the forward scattering peak. In addition, the increase in the concentration also enforces the radiation extinction. These features are correctly captured here. The predicted averaged transmissivity level is 82% (82.0% with the spectral discretization according to 367 bands and 82.1% with the 43 band model), whereas the experimental value given in [4] was 81.4%. This confirms the accuracy of the prediction.

[Figure 2 about here.]

[Figure 3 about here.]

The two previous tests demonstrate our ability to obtain a reference one-dimensional model, which accurately predicts the transmissivity features of the spray in very hard conditions since directional variations are extremely strong. Let us now consider the case of diffuse irradiation when the hemispherical transmissivity is sought. This can be a realistic case, considering that the fire is close to the water curtain. Despite the anisotropy of the scattering, the directional dependence of the intensity is less important since boundary conditions are the same for all directions on the irradiated boundary. This could allow the use of a classical discretization scheme and the application of the global numerical process as described in paragraph 3. A validation will be first presented comparing the corresponding results with data obtained thanks to the reference simulation used for figure 2 and 3 (with the same fine discretization). The width is still $0.24\ m$ and all simulations are in one-dimensional configuration. The hemispherical spectral transmissivity in a given wavelength band is the ratio between the incoming and leaving radiative fluxes at the boundaries of the spray, obtained in the present case following this relation :

$$\overline{T_\lambda} = \frac{2\pi \int_0^1 \overline{I_\lambda}(y=L).\mu.d\mu}{2\pi \int_0^1 \overline{I_\lambda}(y=0).\mu.d\mu} \tag{21}$$

Figure 4 presents the plots of the spectral transmissivity for the cases "TG03 - 1 bar" and "TG03 - 3 bars". Only the 43 band model has been used here since its suitability for the prediction has been proven in the previous Figures. One may observe comparing with Figure 2 and 3, that the transmissivity level is slightly higher, since the loss due to scattering is not as strong as seen before when only directional transmissivity was sought. This is especially true in the short wavelength range where attenuation is mainly due to scattering. This implies that the attenuation ability of the spray is weakened by its too strong forward-scattering feature. Our aim

here was to show that the discrepancy between the two models is very small, therefore validating the use of the complete model presently based on the the so-called $DCT111$ quadrature scheme. When integrating the corresponding results over the whole wavelength range, the difference between the two models in the predicted total transmissivity is around 0.1%.

The present complete formulation has been therefore validated as able to characterize the spray behaviour, without requiring the azimuthal symmetry hypothesis. It may also be extended to the 2D configurations. Let us recall that the present study is planned to be combined with a companion work on the energy balance that will provide non symmetrical temperature fields requiring a 2D solution. In the rest of the paper, all results have been actually computed on 2D cases, where the width is kept as 0.24 m, whereas the second direction corresponds to a heigth equal to 2 m. Results are then presented at a mean vertical position of 1 m, as a function of the horizontal co-ordinate (the main direction for the radiation transfer).

[Figure 4 about here.]

Sensitivity of our complete formulation to some key numerical choices like the difference scheme and the quadrature scheme has been sought. Figure 5 presents some results obtained for the two cases "TG03 - 1 bar" and "TG03 - 3 bars", using two differencing schemes referred as Carlson-Lathrop and step scheme. In fact the discrepancy between the simulations is so small, that we have plotted a relative discrepancy (the difference between the transmissivities predicted with the two proposals (referred as ΔT_λ) divided by the value obtained with the Carlson-Lathrop's scheme), as a function of the wavelength. As can be seen, the difference varies with the wavelength, but never rises up to 4.10^{-3}. Note that tests performed with the diamond scheme resulted in numerical instabilities in the present cases and consequently, this scheme is not represented. Considering relations (19) and (20), large values computed for the radiative properties induce parameters f_y and f_z close to 1 (as in the step scheme). This explains why the step scheme does not fail in the prediction. We keep the Carlson-Lathrop's scheme as the most reliable one, since strong variatons in the spectral behavior of the spray could sometimes affect f_y and f_z, which could be taken into account thanks to relations (19) and (20). Note also that the computational time gained with the step scheme is not significant. Moreover it may induce numerical diffusion in some conditions.

[Figure 5 about here.]

Figures 6 et 7 present a similar task applied on the quadrature scheme. Diffuse irradiation is still considered.

Five quadratures are compared on the "TG03 - 1 bar" case. As can be seen on Figure 6, the discrepancy between the different results may become obvious. The transmissivity prediction seems to be affected by the quadrature whatever the wavelength. Let us recall that the $LC11$ quadrature was mentioned as the most reliable in [13]. This is therefore our reference solution. The $DCT111$ solution is very close to the $LC11$ curve, however. Figure 7 is the same test performed on the "TG03 - 3 bars" case. Three quadrature choices are presented, including the $LC11$ quadrature. As can be seen here again, very little difference is obtained when compared with the $DCT111$, which only uses 80 directions (instead of 120 for the $LC11$). In comparison, the classical S_8 quadrature also uses 80 directions but provides results less close to the quadrature chosen as the reference. Consequently, our basic numerical treatment will be considered as sufficiently reliable and fast, when involving the Carlson-Lathrop's differencing scheme and the $DCT111$ quadrature. In order to complete the present formulation, this quadrature scheme which has been finally chosen, is presented in a table in appendix B.

[Figure 6 about here.]

[Figure 7 about here.]

Figure 8 and 9 show complementary tests aimed at studying if the spray may be well characterized, considering a mean droplet diameter, instead of a complete and detailed size distribution (the pre-processing requirements devoted to the droplet radiative property computations would decrease significantly). The two test cases ("1 bar" and "3 bars") are presented. Various definitions for the mean diameter have been introduced : D_{10} is a simple mean arithmetic diameter based on the droplet diameters and their corresponding density number, D_{20} is based on the square of the diameter (therefore it is a characteristic of the area involved in the interfacial exchanges), D_{30} is based on the cube of the diameter (consequently characteristic of the volume occupied by the droplets) and D_{32} is the Sauter diameter (combining the two latter definitions). The exact definitions are:

$$D_{10} = \frac{\sum_i n_i . d_i}{\sum_i n_i} \; ; \; D_{20} = \sqrt{\frac{\sum_i n_i . d_i^2}{\sum_i n_i}} \; ; \; D_{30} = \left(\frac{\sum_i n_i . d_i^3}{\sum_i n_i}\right)^{\frac{1}{3}} \text{ and } D_{32} = \frac{\sum_i n_i . d_i^3}{\sum_i n_i . d_i^2} = \frac{D_{30}^3}{D_{20}^2} \quad (22)$$

where n_i is the number of droplets having a diameter in the class centred around the value d_i.

The results presented on Figures 8 and 9 show that the use of D_{32} to characterize the whole distribution is a powerful possibility, whereas other mean values are less satisfactory. The maximum discrepancy between the real distribution curve and those obtained using D_{32} has been found to be less than 0.1 % in the "1 bar" case and 0.5% in the "3 bars" case. As a comparison the maximum discrepancy reached with the use of D_{10} in the same conditions was larger than 2 and 9 % respectively. The gain in computational time when using D_{32}

18

can be really important, since radiative properties based on the Mie theory have to be computed once, instead of one time for each size class. Despite this strong cut, the accuracy in the transmissivity prediction remains satisfactory. We do not really recommend such an approach however, since the size distribution is a powerful information source. In the frame of a complete model involving the simulation of the dynamics, the droplet size will be for example a key parameter since the response of the droplets to the flow is expected to strongly vary depending on their inertia (and therefore their size).

[Figure 8 about here.]

[Figure 9 about here.]

5   Water spray curtain characterization

Let us now deal with the study of the actual ability of the spray to weaken the radiative transfer. Transmissivity levels have been observed to remain relatively high in the present simulations (larger than 80% in the "TG03 - 3 bars" case, the most efficient in the present study). One possible way to enhance the attenuation ability is to decrease the droplet size. This has been discussed in the previous article by Berour *et al.* [6]. This is confirmed in the present study where the radiative transfer treatment is improved. Figure 10 is the illustration of the droplet size influence, where hypothetic monosize distributions are considered, keeping the same droplet density than in the "TG03 - 3 bars" case and comparing with the actual polydispersion already presented on Figure 9. As can be seen, transmissivity level may be reduced and attenuation seems to rise as the droplet size is decreased. The total transmissivity reaches for example a minimum value of 55% for the 10 μm droplets. Of course, such a spray would be rapidly dispersed in an open area and would indeed be unable to attenuate the radiation. A compromise has to be found between the radiation extinction ability and the realistic dynamics of the flow.

[Figure 10 about here.]

A second way to improve the radiation attenuation is to enhance the droplet concentration. Tests performed on the "TG03 - 1 bar" and "TG03 - 3 bars" cases are presented on Figures 11 and 12 respectively. Computations have been carried out increasing the number of spray nozzles and therefore the droplet density number. Transmissivities obtained when taking into account the combination of 1, 2, 4 or 8 nozzles are plotted. Considering

the characteristic width of the spray (0.24 m), it corresponds to a nozzle density of 4.2, 8.3, 16.6 and 33.3 nozzles per meter. The dotted line corresponds to the transmission that would be obtained through wet air without any spray (keeping the same moisture, temperature and geometric configuration). It allows to evaluate the respective parts of the attenuation due to the droplets or to the continuous phase. Note that this curve does not reach the 100% level between the absorption bands, as a consequence of losses through the upper and lower boundaries (the analysis is in a 2D configuration, with dimensions 0.24 times 2 m, with diffuse irradiation, so that part of the incident radiation at the boundary defined by $y = 0$ does not leave the computational domain towards the boundary defined by $y = L$). The transmissivity of course decreases with the increase in optical depth which rises with the spray density. The global spectral variations remain similar (due to the continuous phase influence) but the averaged attenuation level varies since scattering and absorption by droplets increase with the number of sprays.

[Figure 11 about here.]

[Figure 12 about here.]

Similar comparisons may be carried out keeping the same size distribution but increasing the spray width. Sprays are added in the main direction of radiation transfer. It does not only enhance the amount of droplets but it also increases the part of the optical depth due to the gas phase. Figure 13 illustrates the drecrease in the transmissivity when the spray width increases. Computations have been carried out for width successively fixed to 0.24, 0.48, 0.72 and 0.96 m, corresponding to the combination "in series" of 1, 2, 3 and 4 nozzles respectively. Comparing with Figure 12, it can be seen that the decrease in transmissivity is faster when such a combination of the sprays is used instead of associating the sprays in parallel in order to enhance the nozzle density. Integrating the transmissivity on the whole wavelength range yielded us a value of 66.7% for curve number 3 of Figure 12 (combination of 4 sprays for a width of 0.24 m to reach the density of 16.6 nozzles per meter) whereas we obtained 49.3% for curve number 4 of Figure 13 (combination of 4 sprays one behind the other with individual width of 0.24 m to reach a global width of 0.96 m). Of course this analysis assumes a constant amount of H_2O and CO_2 in the air whatever the configuration, which is probably not true. Consequently the gain in attenuation when associating the sprays in series is probably overestimated. This is however an interesting point to investigate in a more complete study.

[Figure 13 about here.]

In order to summarize the above results, an equivalent optical depth may be evaluated in each case. For example considering the computed total transmissivity $\overline{T}$ in the various situations and using a Beer's law, the following equivalent optical depth is obtained:

$$\tau = -\ln \overline{T} \tag{23}$$

Comparisons can be carried out in each case with the correlation suggested by Pretrel [3] :

$$\tau_P = \frac{3}{2} . \frac{n.\dot{m}}{V_d L} . \frac{1}{\rho D_{32}} \tag{24}$$

where n is the number of nozzles per curtain meter, $\dot{m}$ is the nozzle mass flow rate and V_d is the mean droplet velocity in the spray.

Figure 14 is a plot where the optical depth τ inferred from the simulation is given as a function of the value τ_P that would be obtained in the same conditions using Pretrel's proposal. All above-discussed results are included. The sign + corresponds to the results of Figure 11 ("TG03 - 1 bar" with increasing nozzle density as the optical depth rises, successively for 4.2, 8.3, 16.6 and 33.3 nozzles per meter). The circles are for the "TG03 - 3 bars" case in the same conditions (as in Figure 12). The triangles are for the monodispersion results (as in Figure 10). The squares correspond to results presented on Figure 13 for the widths 0.48, 0.72 and 0.96 m (with increasing optical depth as the width rises). If a perfect agreement could be achieved between the simulations and the correlation, all symbols would be located on the dotted line. As can be seen, the main parts of the results are shifted above the line. This implies that the correlation tends to underestimate the real optical depth (and hence to underestimate the real radiation attenuation) except in the case of monodispersions of droplets with very small diameters (10 or 20 μm) and in the "TG03 - 3 bars" case when the nozzle density is the highest one. We explain this trend considering that in Pretrel's correlation the attenuation due to the droplets is taken into account, whereas no contribution is attributed to the gas phase itself. On Figure 14 a black circle features the result yielded when no droplets are simulated, keeping the same conditions for the gas phase (with a width of 0.24 m as on Figure 12). The role of the gas phase is obvious, since the simulation predicts an equivalent optical depth, that could at least be taken into account as a corrective term when applying the correlation. Note of course that this correction would be affected by the spray width, which explains why squares are shifting from the dotted line as the spray width is increased. These comments indicate some limitations to the tested correlation, which should be used with care, whereas the present complete simulation could be used as a predicting tool whatever the spray configuration.

[Figure 14 about here.]

6 Conclusion

A complete bidimensional treatment of the radiative transfer inside a water spray curtain, irradiated with a high temperature source, has been tested and validated. The numerical code based on a DOM scheme with a Carlson-Lathrop's closure type, a $DCT111$ quadrature and a c-K model aimed at the spectral desciption, has been observed to be reliable. Comparisons have demonstrated a satisfactory agreement with some experimental data available in the litterature. Provided elementary input data for the features of the spray are given (namely size distribution, relative moisture and temperature) the attenuation capability of the spray may be predicted. In particular, the influence of the nozzle density, the droplet size and the curtain size have been studied. The use of a simple correlation has been proven to yield some possible inaccuracy if no correction is taken into account for the role of the gas phase, unless the nozzle density is really high. The prediction ability of the present code will now be applied on other spray configurations. Of course, the present study has been conducted uncoupled from the other aspects of the problem (namely the energy transfer and the dynamics of the spray). A study of the whole problem combining the various aspects of the simulation is therefore a challenging aim for the coming period.

References

[1] A. Coppalle, D. Nedelka, and B. Bauer. Fire protection : water curtains. *Fire Safety Journal*, 20:241–255, 1993.

[2] S. Dembélé, J.X. Wen, and J.F. Sacadura. Analysis of the two-flux model for predicting water spray transmittance in fire protection application. *ASME J. Heat Transfer*, 122:183–186, 2000.

[3] H. Pretrel. *Étude du comportement thermodynamique de pulvérisations liquides sous l'effet du rayonnement infrarouge. Application à la protection incendie par rideau d'eau.* PhD thesis, INSA de Lyon, 1997.

[4] S. Dembélé. *Modélisation et étude expérimentale des transferts de chaleur par rayonnement dans un rideau d'eau diphasique. Application à la protection incendie d'installations industrielles à risques.* PhD thesis, INSA de Lyon, 1998.

[5] L. Zimmer. *Etude numérique et expérimentale de la turbulence en écoulement gaz-gouttelettes. Applications aux rideaux d'eau en présence de vent latéral.* PhD thesis, Institut Von Karman et UHP Nancy 1, 2001.

[6] N. Berour, D. Lacroix, P. Boulet, and G. Jeandel. Radiative and conductive heat transfer in a non-grey semitransparent medium - application to fire protection curtains. *J. Quant. Spect. Rad. Tran.*, ref 1964-03-028, in press, accepted in June 2003.

[7] A. Soufiani and J. Taine. High temperature gas radiative property parameters of statistical narrow-band model for H_2O, CO_2 and CO, and correlated-k model for H_2O and CO_2. *Int. J. Heat Mass Transfer*, 40(4):987–991, 1997.

[8] B.G. Carlson and K.D. Lathrop. Chap.3, transport theory - the method of discrete ordinates. In *Computing methods in reactors physics*. Gordon and Breach New York, 1968.

[9] M. F. Modest. *Radiative Heat Transfer.* Mc Graw Hill, international editions edition, 1993.

[10] N. El Wakil. *Etude de transferts de chaleur par conduction, convection et rayonnement couplés dans des milieux semi-transparents fluides ou poreux. Elaboration de modèles de simulation en géométrie bidimensionnelle.* PhD thesis, INSA de Lyon, 1991.

[11] S. Chandrasekhar. *Radiative transfer.* Oxford : Clarendon Press, 1950.

[12] D. Lacroix, G. Parent, F. Asllanaj, and G. Jeandel. Coupled radiative and conductive heat transfer in a non-grey absorbing and emitting semitransparent media under collimated radiation. *J. Quant. Spect. Rad. Tran.*, 75:589–609, 2002.

[13] R. Koch and R. Becker. Evaluation of quadrature schemes for the discrete ordinate method. In *Proceedings of Eurotherm 73 on Computational Thermal Radiation in Participating Media*, pages 59–74, 15-17 April 2003.

[14] C.F. Bohren and D.R. Huffman. *Absorption and scattering of light by small particles.* New York : John Willey and Sons, 1983.

[15] R. Koch, W. Krebs ans S. Wittig, and R. Viskanta. Discrete ordinates quadrature schemes for multidimensional radiative transfer. *J. Quant. Spect. Rad. Tran.*, 53(4):353–372, 1995.

7 Appendix A: application of the Mie Theory

The present paper has presented a formulation directly based on the knowledge of the efficiencies and of the phase function for a given particle diameter. Here are recalled the key formulas that yield the numerical values of such properties. Of course, we assume here that the droplets are perfectly spherical with well-kwown constant optical index. Following the formulation by Modest [9] and Bohren and Huffman [14] we successively obtain:

- The extinction efficiency:

$$Q_{e\lambda} = \frac{2}{x^2} \sum_{n=1}^{Nmax} (2n+1).Re[a_n + b_n] \tag{25}$$

- The scattering efficiency:

$$Q_{s\lambda} = \frac{2}{x^2} \sum_{n=1}^{Nmax} (2n+1). \left[|a_n|^2 + |b_n|^2\right] \tag{26}$$

- The absorption efficiency:

$$Q_{a\lambda} = Q_{e\lambda} - Q_{s\lambda} \tag{27}$$

where the Mie coefficients are involved, which may be computed as:

$$a_n = \frac{[D_n(mx)/m + n/x].\psi_n(x) - \psi_{n-1}(x)}{[D_n(mx)/m + n/x].\zeta_n(x) - \zeta_{n-1}(x)} \tag{28}$$

$$b_n = \frac{[mD_n(mx) + n/x].\psi_n(x) - \psi_{n-1}(x)}{[mD_n(mx) + n/x].\zeta_n(x) - \zeta_{n-1}(x)} \tag{29}$$

x is the size parameter defined as the ratio $\frac{2.\pi.r}{\lambda}$ and m is the relative refractive index (complex index of the particle divided by the one of the surrounding medium).

$D_n(x) = \frac{d}{dx} ln\psi(x)$ is a logarithmic derivative. ψ_n and ζ_n are the complex Riccati-Bessel functions, all being possibly computed by stable recurrence relations [14].

The phase function for a particle with given radius r and the scattering angle θ is similarly obtained thanks to a summation:

$$P_\lambda(r,\theta) = 2.\frac{|S_1(\theta)|^2 + |S_2(\theta)|^2}{x^2.Q_{s\lambda}} \tag{30}$$

where S_1 and S_2 are complexe amplitude functions involving the a_n and b_n coefficients:

$$S_1(\theta) = \sum_{n=1}^{Nmax} \frac{2n+1}{n.(n+1)}[a_n.\pi_n(\mu) + b_n.\tau_n(\mu)] \tag{31}$$

$$S_2(\theta) = \sum_{n=1}^{Nmax} \frac{2n+1}{n.(n+1)}[b_n.\pi_n(\mu) + a_n.\tau_n(\mu)] \tag{32}$$

with $\mu = \cos(\theta)$. The series π_n et τ_n are given by:

$$\pi_n = \frac{2n-1}{n-1}.\mu.\pi_{n-1} - \frac{n}{n-1}.\pi_{n-2} \tag{33}$$

$$\tau_n = n.\mu.\pi_n - (n+1).\pi_{n-1} \tag{34}$$

with the following initial values: $\pi_0 = 0$ and $\pi_1 = 1$

Owing to the repetition of summations involving N_{max} terms, this process has sometimes been avoided, authors preferring to apply some approximations. This can no more be a valid argument considering the actual computational ressources. This number is of the order of twice the size parameter of the droplet. In the worst case where the wavelength is 1 μm and the droplet radius 100 μm, this yields $N_{max} = 628$. Actually, in most cases this is an overestimation of the required number of terms. The building of a complete database (involving absorption, scattering coefficients and phase functions for 43 wavelength and the $DCT111$ quadrature) for the here-studied TG03 reference only took 2 minutes on a pentium 4 - 2.4 GHz computer. An exact computation of the radiative properties is consequently easy to perform and has to be introduced in the whole simulation.

8 Appendix B: quadrature scheme $DCT111 - 24681012$

This quadrature scheme has been found here to yield the best compromise between accuracy and low computational time. The corresponding direction cosines and weigths are given in the following table for each node of the first octant, to complete the present formulation.

[Table 1 about here.]

List of Figures

Figure 1: Control volume used in the DOM formulation
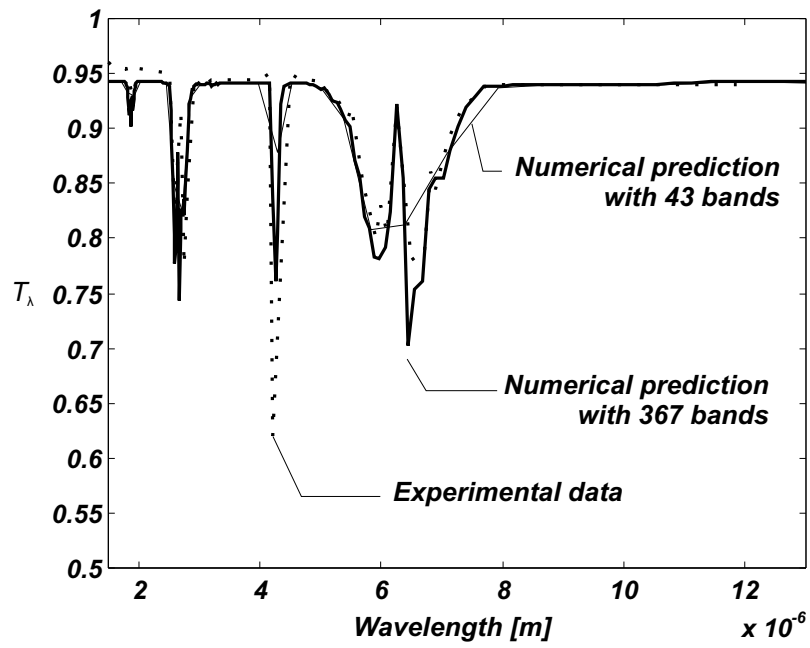
Figure 2: Predicted spectral transmissivity for the "TG03 - 1 bar" case and comparison with the experimental data by Dembélé [4]
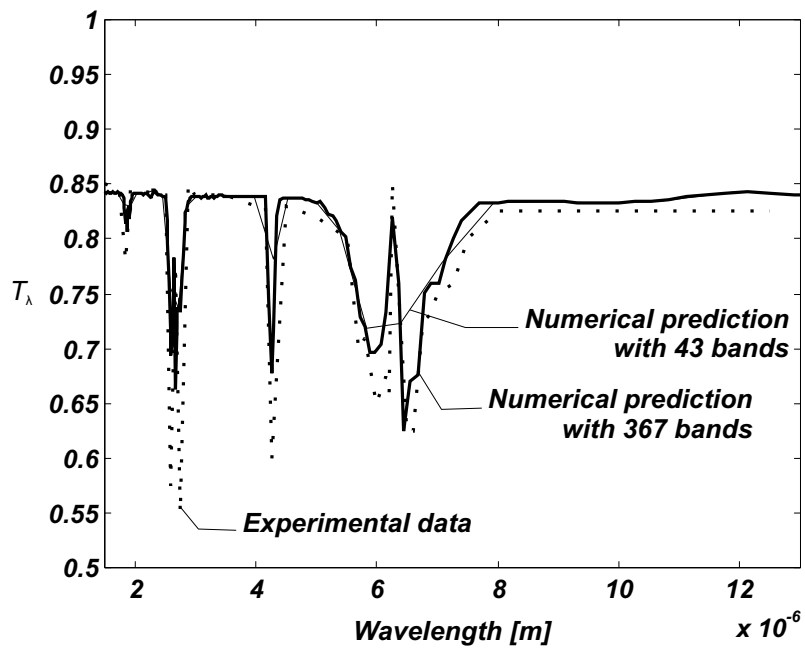
Figure 3: Predicted spectral transmissivity for the "TG03 - 3 bars" case and comparison with the experimental data by Dembélé [4]
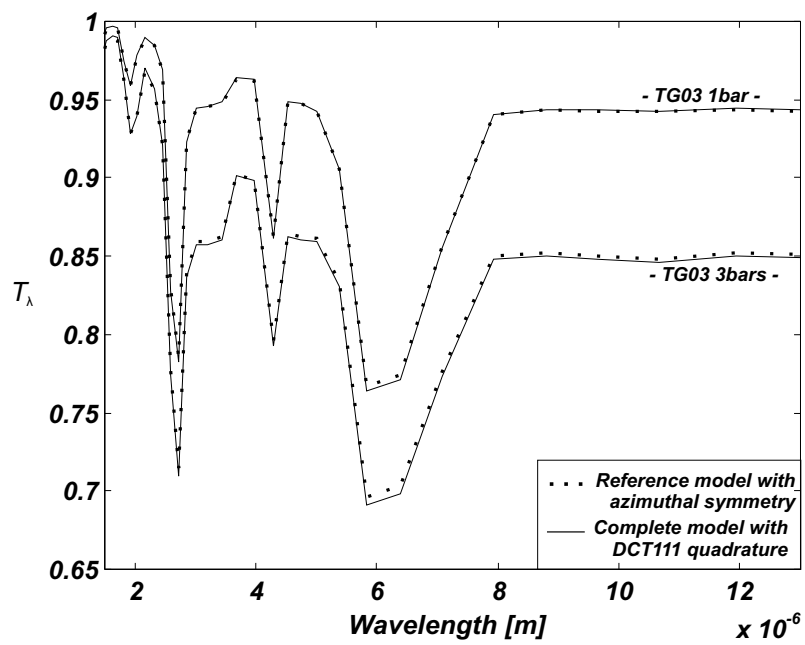
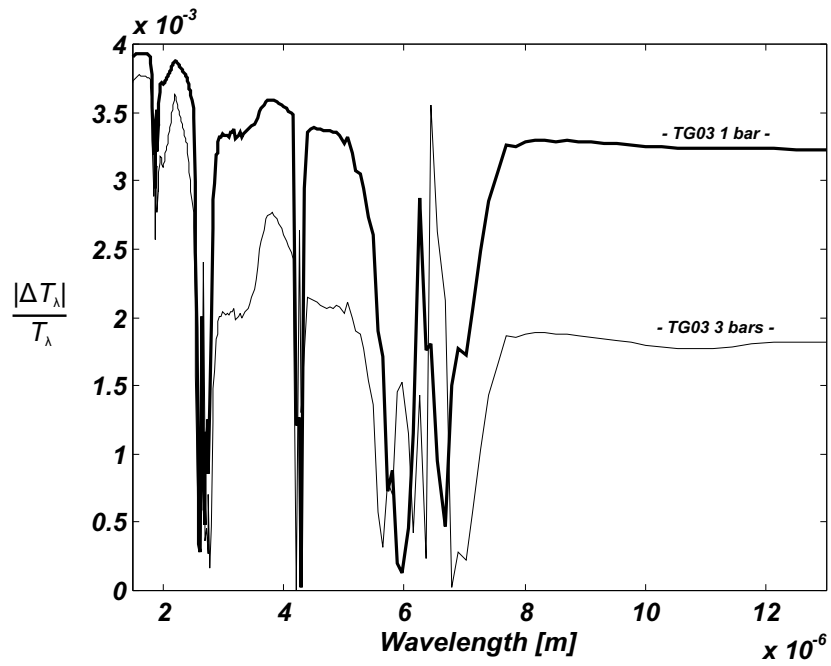Figure 4: Validation of the complete formulation for diffuse irradiation

Figure 5: Discrepancies between the transmissivities yielded by the Carlson-Lathrop's differencing scheme and the step scheme
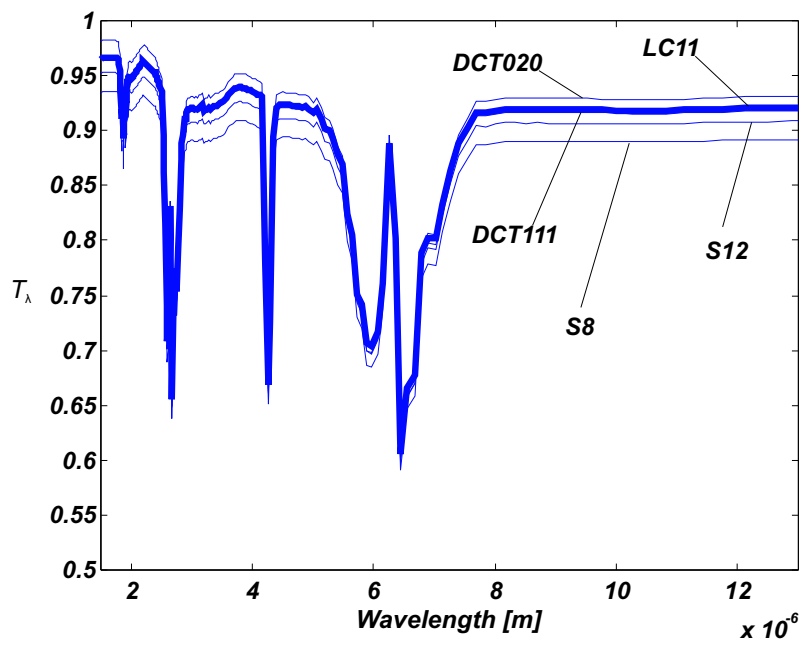
Figure 6: Influence of the quadrature scheme on the predicted transmissivities in the "TG03 - 1 bar" case
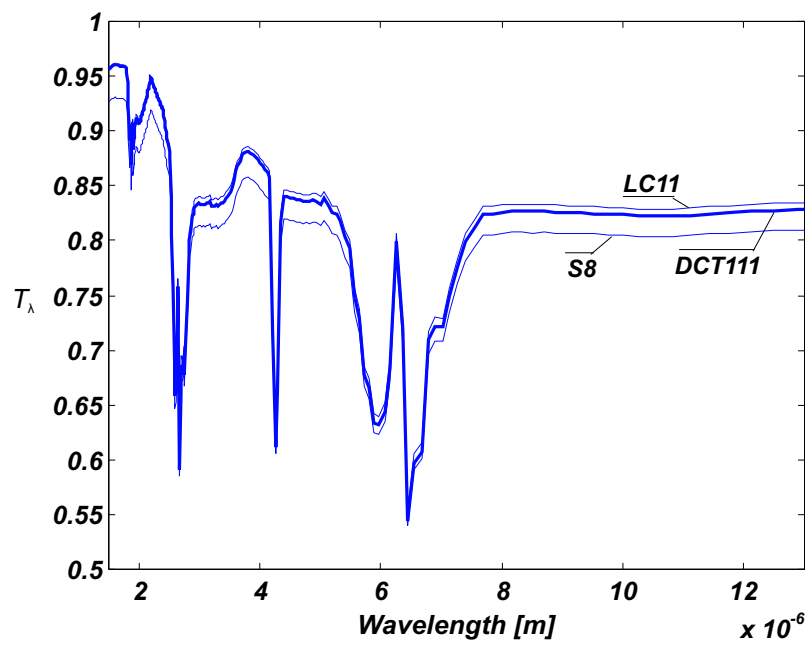
Figure 7: Influence of the quadrature scheme on the predicted transmissivities in the "TG03 - 3 bars" case
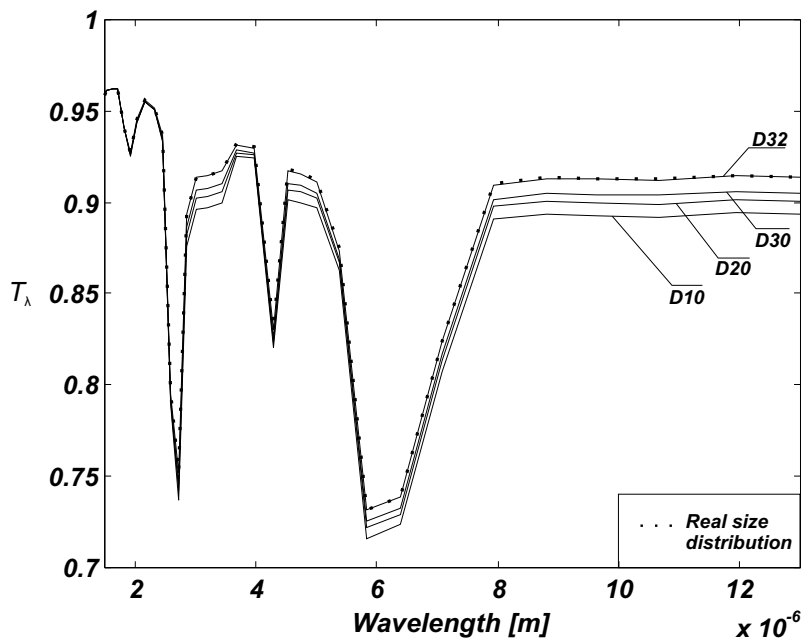
Figure 8: Spectral transmissivities predicted for monodispersions based on various mean diameter definitions, comparison with the real polydispersion result ("TG03 - 1 bar" case)
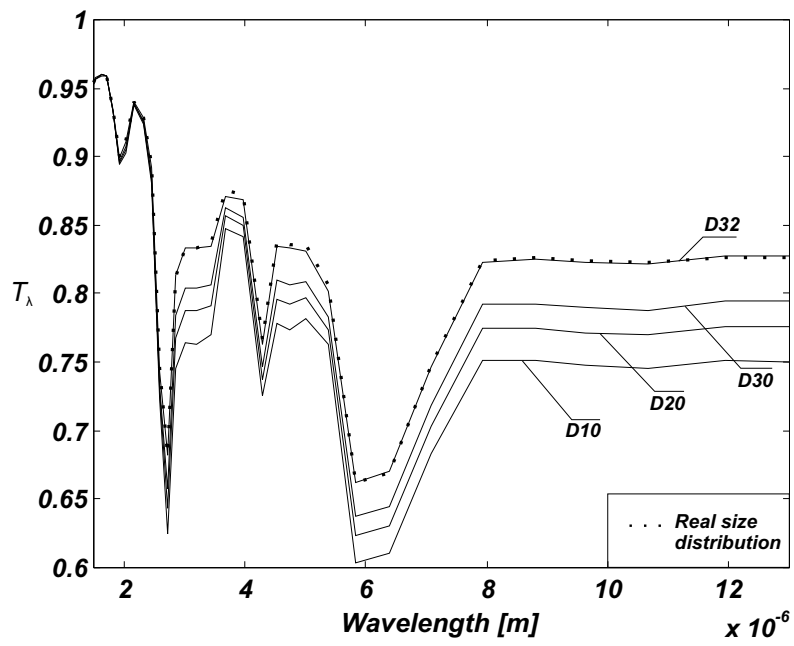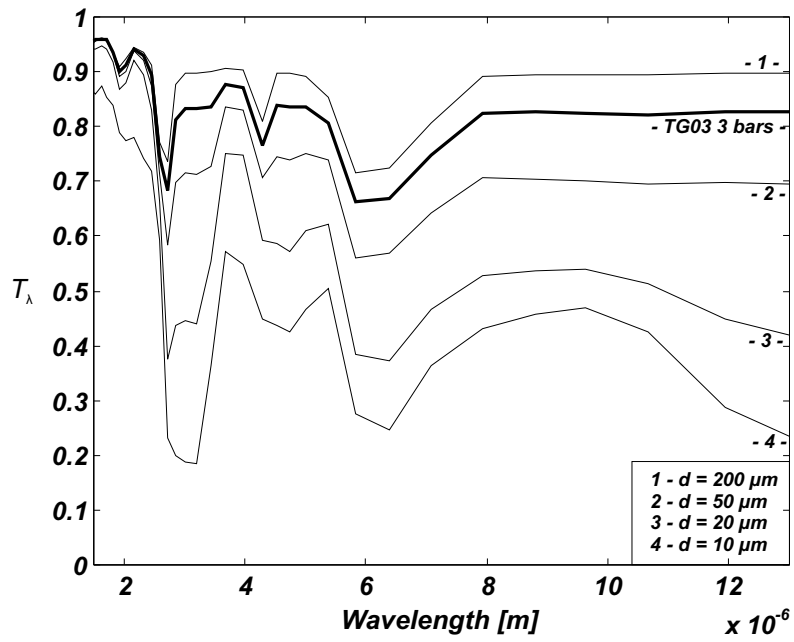
Figure 9: Spectral transmissivities predicted for monodispersions based on various mean diameter definitions, comparison with the real polydispersion result ("TG03 - 3 bars" case)

Figure 10: Spectral transmissivities predicted for various monodispersions and comparison with the "TG03 - 3 bars" case
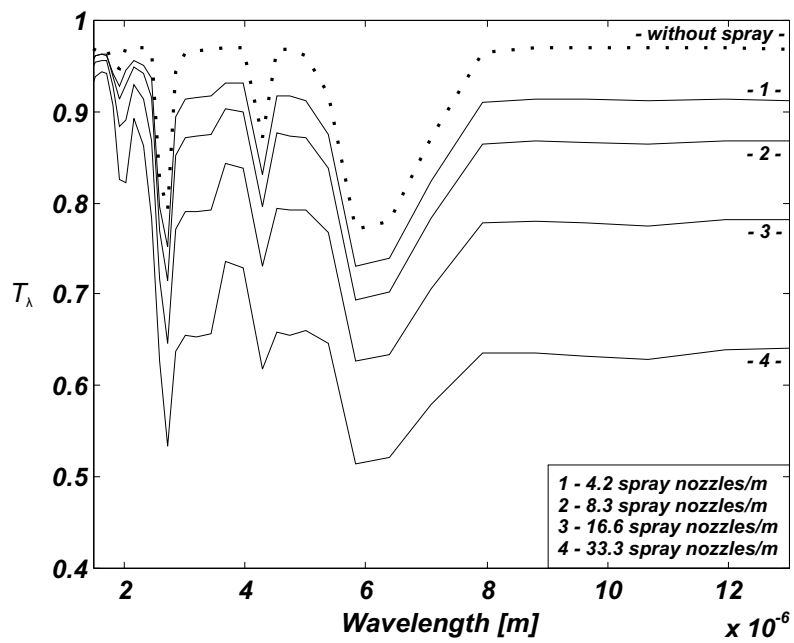
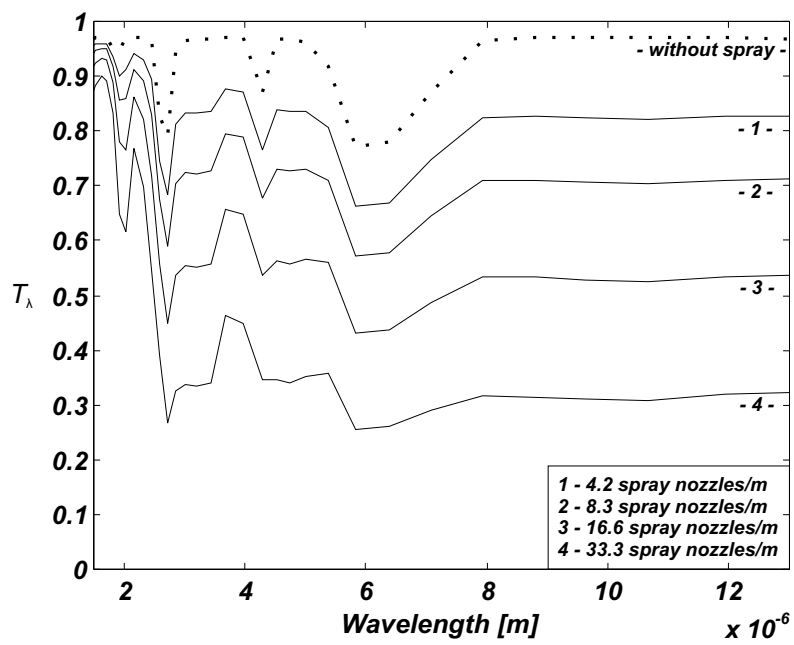Figure 11: Influence of the nozzle density on the spectral transmissivity in the "TG03 - 1 bar" case

Figure 12: Influence of the nozzle density on the spectral transmissivity in the "TG03 - 3 bars" case
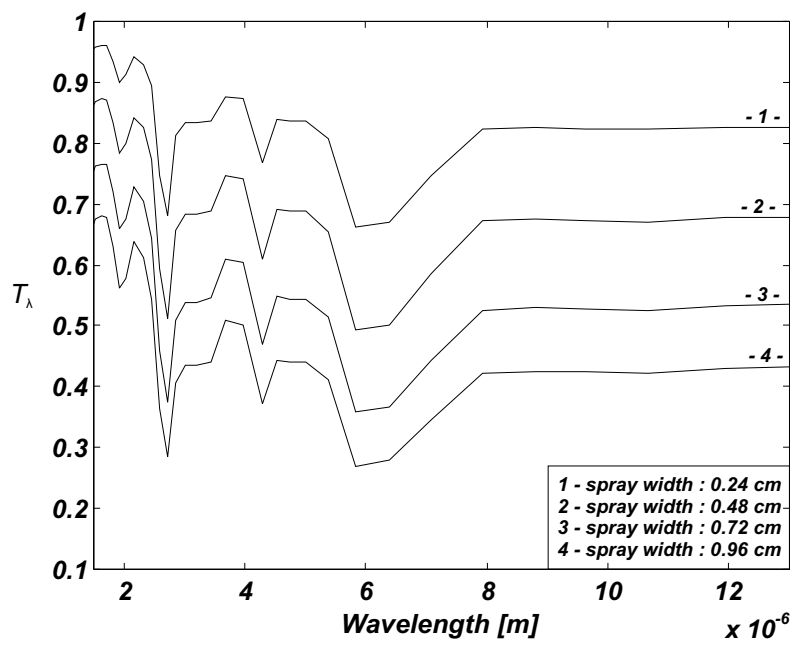
Figure 13: Influence of the spray width on the spectral transmissivity in the "TG03 - 3 bars" case
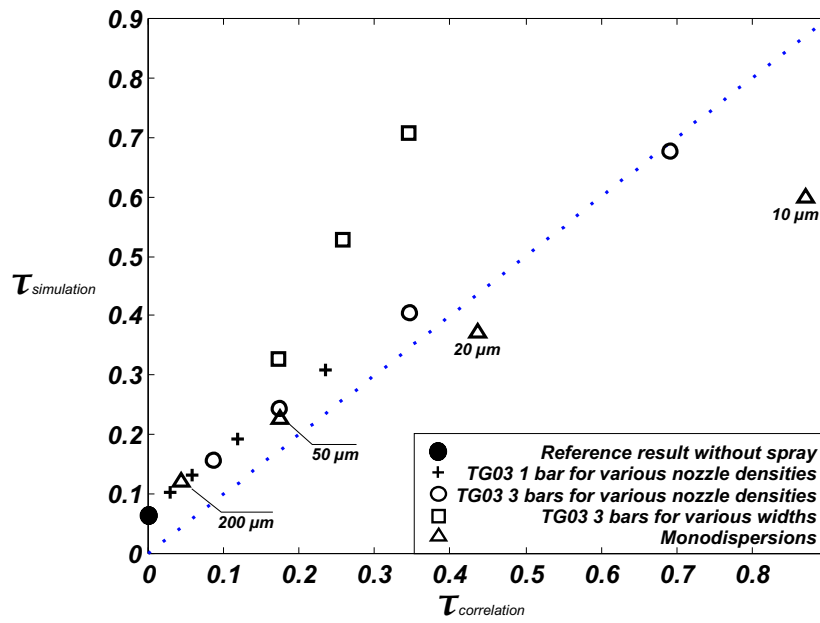
Figure 14: Optical depth deduced from the numerical prediction in various configurations as a function of the value yielded by the Pretrel's correlation [3]

List of Tables

Table 1: Quadrature DCT 111-24681012 according to Koch *et al.* [15]

Node	$\Omega_{x,m}$	$\Omega_{y,m}$	$\Omega_{z,m}$	w_m
1	0.96688413	0.18046478	0.18046478	0.071430026
2	0.81940331	0.20417467	0.53552198	0.192713914
3	0.81940331	0.53552198	0.20417467	0.192713914
4	0.57735027	0.57735027	0.57735027	0.200224182
5	0.53552198	0.20417467	0.81940331	0.192713914
6	0.53552198	0.81940331	0.20417467	0.192713914
7	0.20417467	0.53552198	0.81940331	0.192713914
8	0.20417467	0.81940331	0.53552198	0.192713914
9	0.18046478	0.18046478	0.96688413	0.071430026
10	0.18046478	0.96688413	0.18046478	0.071430026